doi:10.1093/brain/awr119 Brain 2011: 134; 2025–2035 | 2025

BRAIN
A JOURNAL OF NEUROLOGY

Atrophy, hypometabolism and white matter abnormalities in semantic dementia tell a coherent story

Julio Acosta-Cabronero,[1] Karalyn Patterson,[1] Tim D. Fryer,[2] John R. Hodges,[3,4] George Pengas,[1] Guy B. Williams[2] and Peter J. Nestor[1]

1 Herchel Smith Building for Brain and Mind Sciences, Cognition, Memory and Language Group, Neurology Unit, Department of Clinical Neurosciences, School of Clinical Medicine, University of Cambridge, Robinson Way, Cambridge CB2 0SZ, UK
2 Wolfson Brain Imaging Centre, Department of Clinical Neurosciences, School of Clinical Medicine, University of Cambridge, Addenbrooke's Hospital, Hills Road, Cambridge CB2 0QQ, UK
3 Neuroscience Research Australia, Barkers Road, Randwick, NSW 2031, Australia
4 School of Medical Sciences, University of New South Wales, Randwick, NSW 2031, Australia

Correspondence to: Dr Julio Acosta-Cabronero,
Herchel Smith Building for Brain and Mind Sciences,
Cognition, Memory and Language Group, Neurology Unit,
Department of Clinical Neurosciences,
School of Clinical Medicine, University of Cambridge,
Robinson Way, Cambridge,
CB2 0SZ, UK
E-mail: jac@cantab.net

Semantic dementia, in which there is progressive deterioration of semantic knowledge, is associated with focal, typically asymmetric, temporal lobe degeneration. The ventrorostral temporal lobe is most severely affected and there is concordance between atrophy and reduced metabolic activity. In this study, we confirmed the veracity of this claim using ^{18}F-fluorodeoxyglucose positron emission tomography and anatomical magnetic resonance images. The principal aim, however, was to understand the impact on neuronal projections from the ventrorostral temporal cortex lesion by studying the full extent of white matter changes, with no *a priori* assumptions about the nature or spatial location of the tracts involved. Using an unbiased voxel-wise approach known as tract-based spatial statistics, we compared results of whole-brain diffusion tensor imaging—absolute metrics of axial, radial and mean diffusion as well as fractional anisotropy—from 10 patients with mild/moderate semantic dementia and 21 matched controls. Distributions of increased absolute diffusivity and reduced fractional anisotropy for patients with semantic dementia were spatially concordant with each other. Abnormalities in all metrics were highly statistically significant in ventrorostral temporal white matter, more extreme on the left side, thus closely matching results from structural and functional imaging of grey matter. The most sensitive marker of change was radial diffusion. Local white matter tract abnormalities extended rostrally towards the frontal lobe and dorsocaudally towards the superior temporal and supramarginal gyri. To examine more remote changes, we performed a skeletonized probabilistic tractography analysis—'seeding' the rostral temporal voxels identified as abnormal in the patient group—in a healthy control group. Three major neural pathways were found to emanate from this 'seed region': uncinate, arcuate and inferior longitudinal fasciculi. At a less conservative threshold, tensor abnormalities in the semantic dementia group mapped onto the tractographies for the uncinate and arcuate bundles well beyond the rostral temporal lobe; this was not the case for the inferior longitudinal bundle, where abnormalities in semantic dementia did not extend caudal to the atrophic/hypometabolic zone. The results offer direct evidence

Received October 29, 2010. Revised April 8, 2011. Accepted April 11, 2011. Advance Access publication June 6, 2011

for how the ventrorostral temporal lesion, proposed to be responsible for deteriorating semantic knowledge in semantic dementia and separate from 'classic' language areas, is associated with degeneration of efferent white matter projections to such language areas.

Keywords: semantic memory disorders; neurodegenerative mechanisms; diffusion tensor; white matter fibre pathways; tractography
Abbreviations: λ_1 = axial diffusivity; ACE-R = Addenbrooke's cognitive examination–revised; TBSS = tract-based spatial statistics

Introduction

The notion that complex mental faculties might be localized to single, compartmentalized brain regions has probably not been seriously entertained since the early part of the 19th century, when the 'discipline' of phrenology was in fashion. Human abilities such as memory and language must, we now know, arise from the activity of distributed neural networks. The unavoidable implication of this principle is that, in order to discover how the brain achieves such functions and how they go awry when the brain is damaged, we need to understand not only abnormal cortical, grey matter components of the relevant networks, but also the consequences of such lesions for neural pathways: white matter tracts. Progress in this essential arena is now possible because of the development of MRI, and in particular of diffusion tensor imaging; but the story is only beginning to unfold and, as usual, results may differ on the basis of the particular techniques and metrics employed.

The subject of the current study is semantic dementia, a variant of frontotemporal lobar degeneration and arguably the most important current lesion model for understanding semantic memory. Neuroanatomically, semantic dementia is marked by severe temporal lobe degeneration, particularly in the rostral and ventral temporal lobe bilaterally, but often more extreme on the left (Desgranges *et al.*, 2007; Hodges *et al.*, 2010). Cognitively, it is characterized by progressive deterioration of semantic knowledge (Snowden *et al.*, 1989; Hodges *et al.*, 1992). Although the lesion in semantic dementia encompasses a large area of the temporal lobe, the rostral fusiform gyrus bilaterally has been established as a site of maximal degeneration (Chan *et al.*, 2001; Davies *et al.*, 2004; Nestor *et al.*, 2006). Even more compelling, in a recent study using ^{18}F-2-fluoro-2-deoxy-D-glucose-PET, hypometabolism in the rostral fusiform gyri was the only significant neural correlate of the semantic memory deficit, with some evidence for hemispheric specialization according to test material (expressive, verbal: left rostral fusiform; non-verbal, associative: right rostral fusiform) (Mion *et al.*, 2010). Diffusion tensor imaging studies to address white matter tract involvement in semantic dementia are sparse at present (Agosta *et al.*, 2010; Whitwell *et al.*, 2010). Agosta *et al.* (2010) reported that left ventral temporal white matter areas are selectively vulnerable in patients with semantic dementia, with involvement of fibre tracts that extend beyond the temporal lobe. Their results identified degeneration of three major tracts (uncinate, arcuate and inferior longitudinal bundles), relative preservation of the frontoparietal superior longitudinal fasciculus and the genu of the corpus callosum, and total preservation of the caudal corpus callosum. Their analysis employed tractographies targeting predefined language-related 'way-point masks' in the left hemisphere of five patients with semantic dementia. Tract-specific diffusion tensor imaging analyses are only helpful, however, to quantify the overall damage in selected white matter pathways—differential patterns of abnormality within a given tract could not be assessed; furthermore, diffusion tensor behaviours in other fibre bundles were not tested.

The aim of the present study was to provide a novel, comprehensive map of the white matter network changes in semantic dementia across the whole brain. In view of the recent demonstration—after several years of debate—that the neural substrate for semantic memory loss in semantic dementia is localized in the ventrorostral temporal lobe (Mion *et al.*, 2010), we specifically wanted to map the projections of axons originating from this lesion. Diffusion abnormalities in a tract, however, cannot address the directionality of such changes. Therefore, in order to infer tract direction, we adopted a multi-modal imaging approach to compare diffusion changes with both cortical atrophy and hypometabolism. The rationale here is the very plausible assumption that changes in white matter tracts extending between areas of cortical damage and areas of cortical sparing would imply degeneration from the former to the latter. Demonstrating direct concordance between cortical degeneration and white matter abnormalities would, furthermore, validate the diffusion results as being due to tract degeneration, as one would expect a strong coupling between cortical neuronal cell body loss and axonal loss in adjacent white matter.

Materials and methods

Subjects

Ten patients [three females, seven males; mean age (SD) 62.5 (6.5)] with a clinical diagnosis of semantic dementia according to consensus criteria (Neary *et al.*, 1998) were recruited from the memory clinic at Addenbrooke's Hospital, Cambridge, UK. On structural imaging, all had the qualitative pattern of severe rostral peri-fusiform atrophy that was recently suggested to discriminate semantic dementia, as a pathological variant of frontotemporal lobar degeneration, from Alzheimer's disease with disproportionate semantic impairment (Pereira *et al.*, 2009). For the imaging study, 21 control participants [10 males, 11 females; mean age (SD) 69.3 (6.1)] were also recruited and screened to exclude neurological or major psychiatric illness. They performed normally on cognitive screening: mini-mental state examination (Folstein *et al.*, 1975) mean (SD) = 28.8/30 (0.5); and Addenbrooke's cognitive examination–revised (ACE-R, Mioshi *et al.*, 2006) mean (SD) = 94.0/100 (3.7). Written informed consent was

Table 1 Scores on cognitive testing for patients with semantic dementia in this study, and for the age- and sex-matched control participants from Adlam *et al.* (2006) and Pengas *et al.* (2010)[a]

Cognitive measures	Patient										Semantic dementia group	Control group
	1	2	3	4	5	6	7	8	9	10		
MMSE/30	27	27	23	26	25	25	24	22	25	18	24.2 (18–27)	29.2 (25–30)
ACE-R/100	78	77	73	61	60	59	54	52	47	40	60.1 (40–78)	94.4 (86–99)
Rey copy/36	36	36	36	36	34	31	30	34	34	36	34.3 (30–36)	34.2 (31–36)
Rey recall/36	23	11	11	26	12	14.5	12.5	4.5	5.5	15	13.5 (4.5–26)	17.7 (9–27)
Digits-F	6	6	8	7	7	6	6	6	5	7	6.4 (5–8)	6.8 (4–8)
Digits-B	6	5	4	6	5	4	3	4	4	4	4.4 (3–6)	4.8 (3–7)
GNT/30	5	5	2	0	0	0	0	0	0	1	1.3 (0–5)	24.6 (18–29)
Naming/64	50	54	40	21	23	22	12	12	14	1	24.9 (1–54)	62.3 (57–64)
Word–picture matching/64	64	63	55	54	48	40	52	27	33	25	46.1 (25–64)	63.8 (63–64)
CCT/64	56	46	47	44	40	28	47	30	34	41	41.3 (28–56)	59.1 (51–62)
VRLT errors	1	5	1	1	2	2	2	1	2	1	1.8 (1–5)	1.67 (0–5)[a]

Group values are given as mean (range).
ACE-R/100 = Addenbrooke's cognitive examination-revised score out of 100-point total; CCT/64 = Camel and Cactus Test score out of 64-point total; Digits-B = digit-span backwards; Digits-F = digit-span forwards; GNT/30 = Graded Naming Test score out of 30-point total; MMSE/30 = mini-mental state examination score out of 30-point total; VRLT = Virtual Route-Learning Test.

obtained from all the participants and the study was approved by the regional Research Ethics Committee.

The remaining neuropsychological test information for the patients with semantic dementia in this study is presented in Table 1 (for both individuals and as a group) along with appropriate age- and sex-matched control data from a previous study (Adlam *et al.*, 2006). The patients with semantic dementia are ordered in Table 1 on the basis of their scores on ACE-R, from least to most impaired. The Rey Figure (copy and delayed recall; Osterrieth, 1944) and digit span in both directions (digits F and B) refer to the usual versions of these tests. The Graded Naming Test (GNT; McKenna and Warrington, 1983) is a difficult naming test on which most controls do not score at ceiling and on which patients with semantic dementia, who are profoundly anomic, perform very poorly, as Table 1 demonstrates. The subsequent three entries in Table 1 [naming, word–picture matching and the Camel and Cactus Test (CCT; Bozeat *et al.*, 2000)] are the standard semantic measures used in our research in Cambridge: all employ the same 64 objects, half living and half man-made. For naming, each picture (line drawing) is presented on its own and the participant is asked what it is called. For word–picture matching, the participant is shown an array of 10 pictures, the target and nine distractors from the same category; the experimenter names the target picture and asks the participant to point to the matching picture. For the CCT of associative semantic knowledge, the participant sees one target and four response alternatives, all coloured pictures, and is asked to choose the response that is most closely related to the target. The final measure in Table 1, Virtual Route-Learning Test (VRLT), is a topographical memory test that has recently been shown to be highly sensitive and specific in discriminating between patients with Alzheimer's disease, who perform very poorly on this test, and those with semantic dementia who perform well (Pengas *et al.*, 2010).

It is worth noting that, if one chose to sequence the cases with semantic dementia in Table 1 on scores for either naming or word–picture matching, the order of cases would be almost identical to that obtained from the ACE-R scores. This fact reflects—as reported in a number of papers on semantic dementia—how stable and supramodal these patients tend to be in their semantic decline.

Imaging

MRI images were acquired on a Siemens Trio 3 T system (Siemens Medical Systems), equipped with gradient coils capable of 45 mT/m and slew rate of 200 T/m/s, and a 12-channel phased-array total imaging matrix head-coil (Siemens Medical Systems). ^{18}F-2-fluoro-2-deoxy-D-glucose-PET scans were performed on a General Electric Advance scanner (GE Medical Systems). MRI and ^{18}F-2-fluoro-2-deoxy-D-glucose-PET acquisitions took place within 2 weeks of each other for all subjects.

Diffusion tensor imaging

Diffusion data sets were acquired using a twice-refocused, single-shot, echo-planar imaging pulse sequence (Reese *et al.*, 2003): repetition time/echo time/number of excitations = 7800 ms/90 ms/1; matrix, 96 × 96; 63 contiguous axial slices; isotropic voxel resolution of 2 × 2 × 2 mm^3; bandwidth of 1628 Hz/pixel and echo spacing of 0.72 ms. The tensor was computed using 63 non-collinear diffusion directions (b = 1000 s/mm^2) that were maximally spread by considering the minimal energy arrangement of point charges on a sphere (http://www.research.att.com/_njas/electrons/dim3), and one scan without diffusion weighting (b = 0 s/mm^2, b_0). We also allowed for parallel acquisition of independently reconstructed images using generalized, auto-calibrating, partially parallel acquisitions [GRAPPA; (Griswold *et al.*, 2002), acceleration factor of 2 and 39 reference lines].

Volumetric T_1 imaging

T_1-weighted anatomical acquisitions consisted of 3D magnetization-prepared, rapid gradient-echo (MPRAGE) volumes with the following imaging parameters: repetition time/echo time/inversion time/flip angle = 2300 ms/2.86 ms/900 ms/9°, 144 slices, 192 × 192 matrix dimensions and 1.25 × 1.25 × 1.25 mm^3 voxel size. Receiver bandwidth and echo spacing were 240 Hz/pixel and 6.7 ms, respectively.

The entire MRI protocol was acquired during a single 25-min session, and the field of view was systematically aligned in stereotactic space: each brain's anterior commissure–posterior commissure line was

aligned with the axial plane and the interhemispheric fissure was aligned along the sagittal plane at right angles to the coronal plane. In addition to field-of-view's anterior commissure–posterior commissure alignment, to maximize acquisition consistency across subjects, the scanning bed was adjusted accordingly to match the scanner isocentre with the centre of the thalamus in the mid-sagittal plane.

^{18}F-2-fluoro-2-deoxy-D-glucose-positron emission tomography

^{18}F-2-fluoro-2-deoxy-D-glucose-PET scans—preceded by a 6 h fast—were obtained in 3D mode. Subjects were scanned in a dimly lit, quiet room, without using earplugs and blindfolds; the subjects were at rest, but not sleeping. A 15-min transmission scan for attenuation correction was performed in 2D mode using rotating ^{68}Ge rods, and then a 150 MBq fluoro-2-deoxy-D-glucose intravenous bolus injection was given over 30 s. PET-emission images were obtained 35–55 min after injection, and were reconstructed using the PROMIS 3D filtered back projection algorithm (Kinahan and Rogers, 1989) into 128 × 128 × 35 arrays with voxel size 2.34 × 2.34 × 4.25 mm^3. Note that corrections were applied for dead time, randoms, normalization, scatter, attenuation and decay.

Data processing and analysis

Diffusion tensor imaging

Until recently, diffusion tensor imaging studies of patients mostly focused on changes in fractional anisotropy. This choice is based on the assumption that neuronal loss will be captured by unequal changes in radial compared with axial diffusion, causing loss of anisotropy in the shape of the diffusion ellipsoid. Empirical neurobiological evidence for fractional anisotropy as the most appropriate metric is, however, lacking. Regarding the various measures of diffusivity, we recently reported—using the same acquisition parameters as in the present study—that fractional anisotropy failed to capture changes in Alzheimer's disease (Acosta-Cabronero *et al.*, 2010). Exploring the full tensor revealed that axial diffusivity (λ_1), radial diffusivity and mean diffusivity were far more sensitive than fractional anisotropy. Although changes in λ_1 were marginally greater than those in radial diffusivity and mean diffusivity for patients with Alzheimer's disease, axial and radial diffusion increased fairly similarly in the white matter areas affected by disease, thus reducing the potential for fractional anisotropy to reveal abnormality. It does not follow, however, that this conclusion would apply to all neurodegenerative diseases: differing degrees of neuronal and glial pathology, apoptosis, inflammation, etc., in different diseases could give rise to different behaviours. It is even possible that such tensor behaviours (varying patterns in λ_1, radial diffusivity, mean diffusivity and fractional anisotropy) could have disease specificity.

Tract-based spatial statistics

The functional MRI of the brain (FMRIB) software library (FSL v4.1) (Smith *et al.*, 2004) was employed to process and analyse diffusion tensor imaging data. First, each diffusion-weighted volume was affine-aligned to its corresponding b_0 image using the FMRIB's linear image registration tool (FLIRT v5.4.2) (Jenkinson and Smith, 2001); this preprocessing step corrects for motion artefacts and eddy-current distortions. Prior to fitting the tensor, brain masks of each b_0 image were generated using the brain-extraction tool (BET v2.1 or BET2) (Smith, 2002) with fractional threshold, $f = 0.1$, and vertical gradient, $g = 0$. BET is based on regional properties of the image, where the forces pushing the template outward are locally computed at each vertex. The FMRIB's diffusion toolbox (FDT v2.0) was then used to fit the tensor and compute the diagonal elements (λ_1, λ_2 and λ_3) at each brain voxel, from which fractional anisotropy, radial diffusivity and mean diffusivity were subsequently inferred.

The tract-based spatial statistics (TBSS v1.2) approach (Smith *et al.*, 2006), whereby the nearest most relevant tracts in each subject's spatially normalized fractional anisotropy image are projected onto a skeleton, was used to perform voxel-wise statistics at the tract centres only, hence minimizing the effect of misregistration—a common problem that is compounded by atrophy.

Spatial normalization was performed by choosing a target image i.e. the map that required the least amount of non-linear warping to match all other images, which was then affine-aligned into MNI152 standard space (Montreal Neurological Institute). The combination of the two transformations was applied to each subject's fractional anisotropy image, and all (i.e. patients and controls) warped fractional anisotropy maps were then averaged to create the mean fractional anisotropy template, from which the mean fractional anisotropy skeleton was derived. Finally, all subjects' normalized fractional anisotropy, λ_1, radial diffusivity and mean diffusivity data were projected onto the skeleton and fed into voxel-wise statistics.

TBSS uses permutation-based non-parametric inference on unsmoothed statistical maps; 10 000 permutations of the data were generated to test against using 'randomize v2.1', and cluster-like structures were enhanced using the threshold-free cluster enhancement algorithm (Smith and Nichols, 2009). The statistical maps were corrected for multiple comparisons, with the threshold level set to family-wise error-corrected $P < 0.05$.

Skeletonized probabilistic tractography

The abnormal skeletonized voxels inferred from the most sensitive diffusion tensor imaging metric were used to 'seed' the tractography algorithm. The most extensive TBSS result was de-projected onto each control subject's native diffusion tensor imaging space to generate subject-specific 'seed masks'.

The probabilistic diffusion tractography algorithm (probtrackx) implemented in FMRIB's diffusion toolbox v2.0 allows the computation of 'connectivity' distribution maps. The algorithm uses the uncertainties inferred from resolving the principal diffusion direction at each voxel to estimate the probability that a pathway passing through a 'seed voxel' will also pass through any other brain voxel (Behrens *et al.*, 2003*b*). The model also incorporates a solution to the multiple-fibre orientation problem (bedpostx) (Behrens *et al.*, 2007).

In this study, 5000 distance-corrected probabilistic pathways were computed using modified Euler integration for each 'seed voxel'. Fractional anisotropy and curvature (cosine of the minimum allowable angle: 0.2, or ~80°) stopping criteria were imposed; pathways were also terminated after 2000 steps, using a step length of 0.5 mm.

Tractographies computed for each control subject were projected back onto the spatially normalized skeleton using the projection vectors inferred from the original fractional anisotropy data, and were then averaged. The resulting skeletonized 'connectivity' distribution map was finally thresholded to confine it to probabilities only >1% of the maximum possible number of probabilistic pathways in a voxel, i.e. 5000 × total number of 'seed voxels'.

Voxel-based morphometry

SPM5 (http://fil.ion.ac.uk/spm) is a frequently employed voxel-wise method for evaluating regional differences in grey matter density, i.e. atrophy, using a technique known as voxel-based morphometry (Ashburner and Friston, 2000). SPM5, which was used with its default settings, enables non-linear warping to MNI152 standard space, tissue

classification and radio-frequency bias correction to be combined within its model (Ashburner and Friston, 2005). The resulting warped grey matter segments were modulated to compensate for the volumetric differences introduced by warping, and smoothed using an 8-mm full width at half-maximum isotropic Gaussian kernel. Recent studies, however, have shown that skull stripping and radio-frequency bias correcting magnetic resonance images can improve the performance of warping algorithms (Fein *et al.*, 2006; Acosta-Cabronero *et al.*, 2008; Pereira *et al.*, 2010). Scans were therefore preprocessed prior to processing in SPM5 by the following automated pipeline: first, skull-stripping was performed using the hybrid watershed algorithm (Segonne *et al.*, 2004) in FreeSurfer v3.04 (http://surfer.nmr.mgh.harvard.edu). The hybrid watershed algorithm makes use of local statistics for the template deformation and integrates an atlas-based term constraining the shape of the brain. Stripped volumes were then bias corrected using the non-parametric, non-uniform intensity normalization algorithm or N3 v1.10 (Sled *et al.*, 1998) with default arguments. N3 corrects intensity non-uniformities without requiring a model of tissue classes; instead, it uses a deconvolution kernel to sharpen the histogram plots that have been smoothed by the bias field. And finally, fine brain extraction that further excludes venous sinuses and CSF prior to SPM5 was performed using BET2 with fixed arguments: $f = 0.2$ and $g = 0$. Preprocessing and warping procedures need reasonable initial estimates; hence the origin of each structural volume was set manually to the anterior commissure prior to preprocessing.

Non-parametric statistics using 'randomize' were then used to perform the group comparison; 10 000 permutations of the data were generated to test against. The threshold level was set to family-wise error-corrected $P < 0.05$.

^{18}F-2-fluoro-2-deoxy-D-glucose-PET data processing and voxel-wise analysis

Mean (35–55 min) emission maps were generated and their origins were also set to the anterior commissure. The resulting volumes were skull stripped using BET2 ($f = 0.7$, $g = 0$), rigidly aligned to their corresponding preprocessed structural image, and resliced (sinc interpolated) to match the sampling of structural volumes using the VTK CISG registration toolkit v2.0.0 (Rueckert *et al.*, 1999). Aligned, resampled, mean emission maps were then transformed into stereotactic space using the SPM5 warp transforms of preprocessed structural volumes, and resampled to 2-mm isotropic voxels using seventh-degree *b*-spline interpolation. Finally, mean emission maps in MNI standard space were normalized to the total mean (including patients and controls) of primary sensory–motor cortex [Brodmann areas (BAs) 1, 2, 3 and 4] radioactivity concentration (Mion *et al.*, 2010), and were smoothed with a 16-mm full width at half-maximum Gaussian kernel.

Consistent with the above TBSS and voxel-based morphometry analyses, 10 000 random permutations of the ^{18}F-2-fluoro-2-deoxy-D-glucose-PET data were also performed using 'randomize', and a threshold level of family-wise error-corrected $P < 0.05$ was applied to determine significant ^{18}F-2-fluoro-2-deoxy-D-glucose-PET differences between patients with semantic dementia and healthy elderly controls.

3D visualization

3D data sets, such as templates, thresholded statistical maps and skeletonized tractographies were rendered using the Mayavi engine (http://code.enthought.com/projects/mayavi). Mayavi was scripted from Python and used the VTK library for its visualization tasks via Traited VTK (TVTK).

Results

As expected, significant atrophy and hypometabolism were observed in the rostral and inferior temporal lobes of the patients with semantic dementia, more extreme on the left than the right. Diffusion tensor abnormalities—as illustrated by the distribution of increased radial diffusivities in semantic dementia—were concordant with the structural and metabolic data (Fig. 1). The composite rendering clearly indicates the agreement across imaging modalities.

TBSS results for decreased fractional anisotropy and increased diffusivities in patients with semantic dementia overlaid onto the MNI152 template and the mean fractional anisotropy skeleton (Fig. 2) confirmed that white matter damage in semantic dementia is predominantly associated with inferior anterior temporal lobe neurodegeneration. Anisotropy and absolute diffusion abnormalities showed overall concordance with each other, but differences in radial diffusivity were the most widespread.

TBSS results for increased radial diffusivity in patients with semantic dementia at a less stringent threshold (uncorrected, $P < 0.01$) highlighted the involvement of connections to frontal areas through the uncinate and arcuate fasciculi, and strong left lateralization, particularly in connections to superior temporal and supramarginal gyri (Fig. 3).

The average-control, skeletonized tractography 'seeded' with abnormal radial diffusivity voxels in semantic dementia (Fig. 4) features pathways: (i) to the orbitofrontal region through the uncinate fasciculus; (ii) to the frontal lobe (via the superior temporal gyrus) through the arcuate fasciculus; and (iii) to the occipitotemporal regions through the inferior longitudinal fasciculus. TBSS results for increased radial diffusivity in patients with semantic dementia at the uncorrected threshold level revealed abnormalities extending further rostrally and dorsally through the uncinate fasciculus and arcuate fasciculus remote from the most severe alterations, but not further caudally through the inferior longitudinal fasciculus (Fig. 4). All other diffusion tensor imaging metrics revealed the same remote alterations (at an uncorrected threshold level) along the uncinate and arcuate fasciculi (data not shown).

Discussion

There was high concordance in the distributions of atrophy and hypometabolism in the temporal cortex of patients with semantic dementia (Fig. 1). This result replicates a previous study comparing these imaging modalities (Desgranges *et al.*, 2007). The novel contribution of the current study was a TBSS analysis offering an unbiased whole-brain view of the landscape of white matter tract degeneration in semantic dementia. The results of this analysis provide yet more concordance: the principal white matter abnormalities closely mirrored the regions of structural and metabolic abnormalities in the cortex; this is most obvious from the comparison of the findings from each imaging modality (Fig. 1). Aside

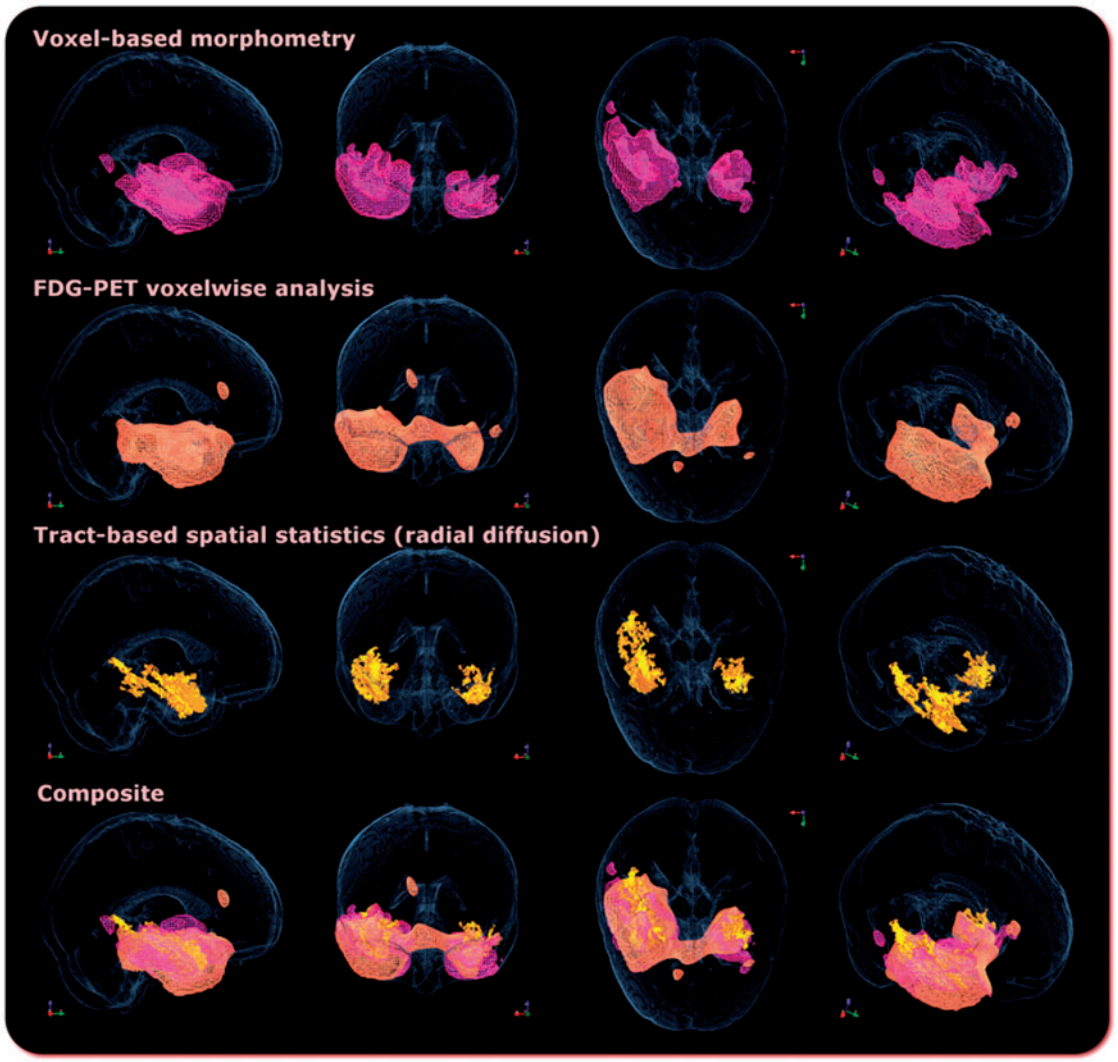

Figure 1 Non-parametric statistical results of reduced regional grey matter density (*top* row 1), reduced mean ^{18}F-2-fluoro-2-deoxy-D-glucose-PET (row 2), increased radial diffusivity (row 3) and a composite of the first three (*bottom* row 4) for 10 patients with semantic dementia compared with 21 healthy controls, all at family-wise error-corrected $P < 0.05$.

from reinforcing the focal nature of ventrorostral temporal lobe degeneration in semantic dementia, this tight coupling of diffusional white matter changes with two markers of grey matter degeneration offers strong evidence that diffusion tensor imaging in degenerative disease is a marker of axonal loss. This last point has been largely assumed, but was lacking in evidence: in principle, diffusion abnormalities could be driven by, for instance, glial changes. All four diffusion metrics detected broadly concordant abnormalities in the temporal lobes, though radial diffusivity showed greatest sensitivity (discussed further below).

The contrast between the uncorrected TBSS results for patients with semantic dementia and the average tractography from age-matched controls revealed that the abnormality identified in the statistically stringent analysis tracked into the uncinate and arcuate fasciculi, extending beyond the atrophic and hypometabolic temporal lobe regions (Fig. 3). With one notable exception, these results are in close agreement with the diffusion study by Agosta *et al*. (2010) that employed a different methodology: Agosta *et al*. (2010) also reported significant inferior longitudinal fasciculus involvement in semantic dementia, not replicated in our data. This discrepancy may be explained by the differing methodologies. Agosta *et al*. (2010) used tractographies to create regions of interest and then studied the diffusion metrics within these masks. A significant change in diffusion measures could have been generated, therefore, either from all voxels within the region of interest, or from a subset of abnormal voxels that changed the mean for the whole region. We suggest the latter as the likely explanation because, in our results, inferior longitudinal fasciculus involvement was restricted to the rostral temporal lobe and did not extend into the cortically uninvolved occipital lobe.

A white matter pathway can receive fibres from multiple grey matter regions; this phenomenon can be modelled by probabilistic tractography algorithms (Behrens *et al*., 2003*a*, 2007). Abnormal white matter pathways, as measured with TBSS, can therefore be

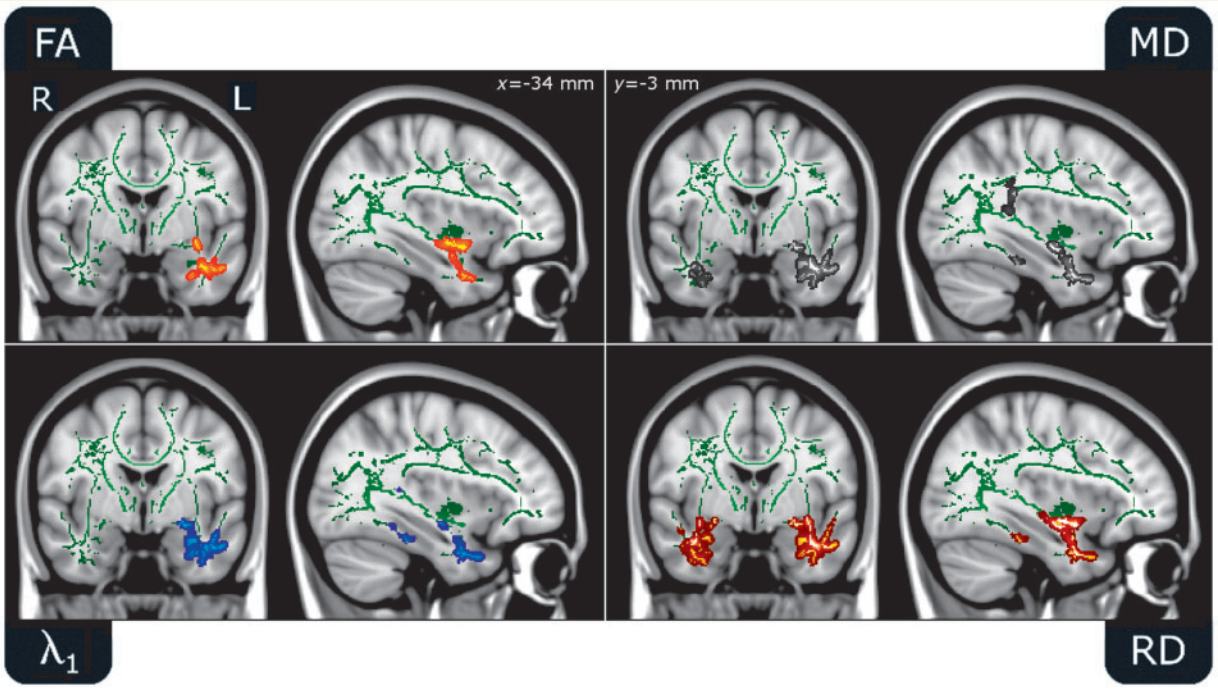

Figure 2 Thresholded TBSS maps for reduced fractional anisotropy (FA) and increased λ_1, radial diffusivity (RD) and mean diffusivity (MD) in 10 patients with semantic dementia compared with 21 controls at family-wise error-corrected $P < 0.05$. All metrics were abnormal in inferior temporal white matter areas.

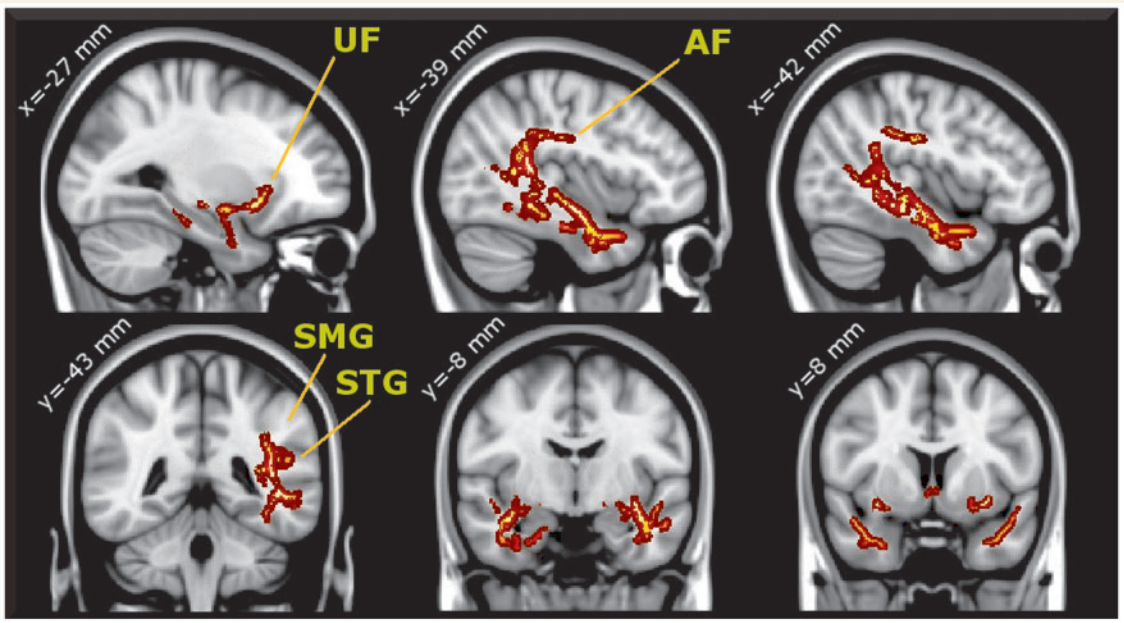

Figure 3 TBSS results for increased radial diffusivity in patients with semantic dementia compared with controls at uncorrected $P < 0.01$. AF = arcuate fasciculus; SMG = supramarginal gyrus; STG = superior temporal gyrus; UF = uncinate fasciculus.

the result of axonal degeneration in certain—but not all—cortical regions that contribute to a tract. This scenario is exemplified by the inferior longitudinal fasciculus involvement detected only in anterior temporal areas, where inferior longitudinal fasciculus fibres merge those from uncinate and arcuate bundles. Another critical point about tractography is that it cannot determine the direction of axonal projections in a tract. Here, though, information about the location of the cortical lesion obtained by ^{18}F-2-fluoro-2-deoxy-D-glucose-PET and structural MRI becomes relevant. With this additional information, we interpret the finding

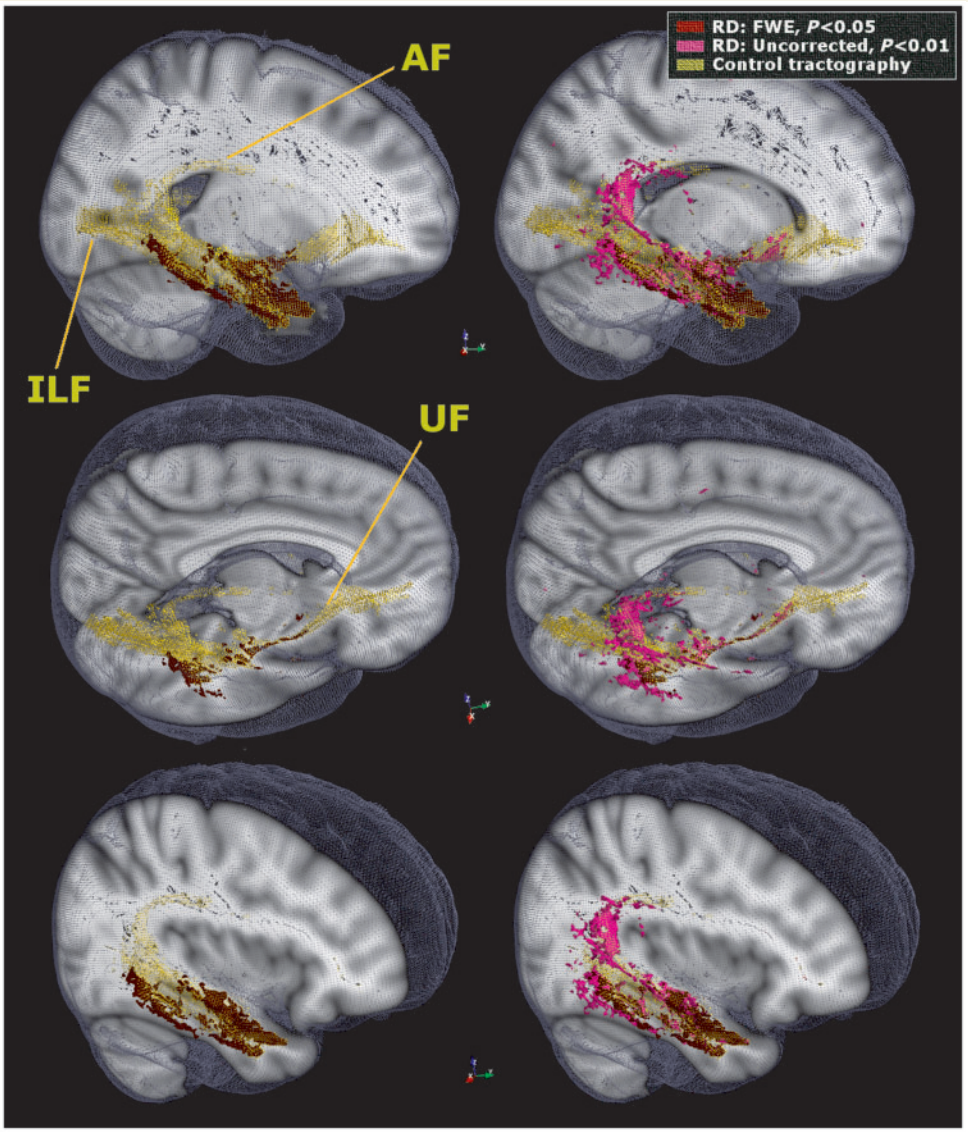

Figure 4 White matter tract abnormalities in patients with semantic dementia projected onto a control tractography highlights: (i) the involvement of the arcuate and uncinate bundles; and (ii) the sparing of tracts running caudally from the temporal lobe through the inferior longitudinal fasciculus. AF = arcuate fasciculus; FWE = family-wise error; ILF = inferior longitudinal fasciculus; RD = radial diffusivity; UF = uncinate fasciculus.

as one of preservation of feed-forward inferior longitudinal fasciculus fibres departing from the occipital lobe, while suggesting that neuronal cell body degeneration in rostral temporal grey matter impacts on projections into the uncinate and arcuate fasciculi. In other words, the findings for inferior longitudinal fasciculus, arcuate and uncinate bundles, when combined with the ^{18}F-2-fluoro-2-deoxy-D-glucose-PET and structural MRI results, indicate that projections that can be considered as predominantly efferent from the damaged temporal lobe (arcuate and uncinate) are degenerating, but those that are predominantly afferent (inferior longitudinal fasciculus) into this region are relatively preserved. This interpretation may seem at odds with known feedback neurons along the ventral stream that, presumably, would be degenerating in semantic dementia. However, it is important to consider that tracts do not simply run between two points but are rather constantly giving off and gaining new axons. We propose that feedback neurons—emanating from the degenerated zone—would likely be projecting to cortex all along the ventral stream, such that the occipital part of the inferior longitudinal fasciculus would contain proportionally few feedback neurons that had originated in the rostral temporal lobe (Fig. 5).

This conceptualization bears some relevance to the ongoing debate about how the brain supports semantic knowledge. A wealth of functional MRI studies in normal participants report that tasks requiring access to semantic representations of objects activate sensory and motor regions corresponding to the perception of and action upon these same objects. Neuropsychological studies in semantic dementia, however, suggest that the temporal

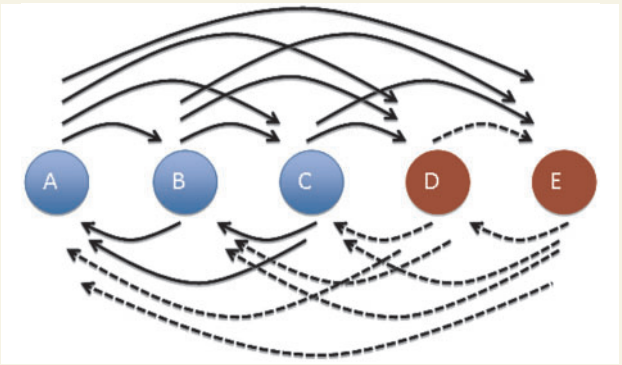

Figure 5 Graphical interpretation of inferior longitudinal fasciculus involvement. Circles represent points along cortex (A = most caudal; E = most rostral; blue = spared; red = pathological). Arrows represent axons in white matter (solid = spared; dashed = pathological). Feed-forward and feed-back projections have been separated for clarity (above and below, respectively). Note that the model predicts proportionately less abnormality in white matter as one moves caudally.

lobe lesion causes a deficit in semantic processing in all modalities (Patterson *et al.*, 2007). This well-established finding has led to a proposal that the rostral temporal lobe might represent a 'hub' that links all the disparate elements of a semantic concept—for instance, that an apple is a fruit; is round and of a particular size; has a certain taste; can be made into cider; is associated with William Tell, New York City and Isaac Newton; and so on. Both the directionality (that information passes forward from sensory areas) and its destination (converging on the rostral temporal lobe) were illustrated in a study using magnetoencephalography: a task in which participants made semantic judgements to spoken or written words initially activated the respective modality-specific auditory and visual brain areas, but activation then later converged on the rostral temporal lobe (Marinkovic *et al.*, 2003). The recent finding that the semantic deficit in semantic dementia is underpinned by a relatively focal lesion to the rostral fusiform gyri (Mion *et al.*, 2010) suggests a particularly focal location for this putative 'hub'. The finding in the current study that the inferior longitudinal fasciculus, which could be viewed as a conduit for visual object information, is uninvolved caudal to the degenerated rostral temporal lobe adds further evidence that semantic dementia is a disorder of the integration of these disparate elements to form a semantic concept. This notion is further supported by the observation that patients with semantic dementia have no difficulty recognizing a perceptually identical exemplar of an object that they have seen before, but are significantly impaired if the new stimulus is a different exemplar of the same object type, or even if it is the same, but presented in a different colour or from a different angle (Graham *et al.*, 2000; Ikeda *et al.*, 2006).

The finding of arcuate fasciculus involvement warrants special mention. Agosta *et al.* (2010), who, as already noted, also identified this abnormality, highlighted an apparent paradox in that arcuate lesions are thought to be synonymous with word-repetition deficits—as seen in conduction aphasia—yet preserved single-word repetition is a characteristic feature of semantic dementia. Here we propose that the combined results of the cortical lesion mapping (^{18}F-2-fluoro-2-deoxy-D-glucose-PET and structural MRI) and diffusion tensor imaging offer a solution. Again it is important to highlight the fact that tracts receive inputs from multiple cortical regions. Therefore, identifying a lesion in a given tract is not evidence that all fibres of that tract are damaged. Previous tractography work localized fibres of the arcuate fasciculus that link posterior superior temporal gyrus and adjacent inferior parietal areas such as the supramarginal gyrus (collectively, 'Wernicke's area') to the ventrolateral frontal lobe ('Broca's area') (Catani *et al.*, 2005). A lesion to this connection is widely considered to be the basis of impaired repetition in conduction aphasia. Although the current results indicate that the ventrorostral temporal lobe also sends a projection into the arcuate fasciculus, consistent with white matter tract dissection in humans (Ture *et al.*, 2000), the ^{18}F-2-fluoro-2-deoxy-D-glucose-PET and structural imaging yielded no evidence of primary damage to the 'classic' posterior language areas (posterior superior temporal gyrus, supramarginal gyrus), the ventrolateral frontal lobe, nor of the white matter connections between these two regions. Preservation of this pathway predicts that patients with semantic dementia should succeed in repeating single-spoken words, even those for which they have no understanding; this, in turn, is precisely the pattern that has been documented in semantic dementia (Hodges *et al.*, 2008). Uncinate fasciculus involvement was also found—this tract connects the rostral temporal lobe with the ventral frontal lobe, hence this was unsurprising. As to whether this lesion has an impact on semantic processing remains unclear presently; it has been proposed to be a component of the semantic network (Vigneau *et al.*, 2006) and the current findings at least indicate the possibility of it being relevant to semantic dementia.

We propose, however, that the key finding of the current study was not the uncinate, arcuate and inferior longitudinal fasciculus results, but instead, the local changes that would not have been captured by focusing exclusively on the former major tracts. For example, there was contiguous involvement of white matter pathways leading from the severely degenerated ventrorostral temporal lobe to the supramarginal gyrus and the posterior superior temporal gyrus (Fig. 3)—in other words, to the 'classic' posterior language areas, which, as discussed above, are themselves spared (as demonstrated by the structural and metabolic results). We interpret these changes as representing degeneration of axons whose cell bodies arise in the former and project to the latter. This finding offers direct evidence of how the ventrorostral temporal lesion—most notably the anterior fusiform (Binney *et al.*, 2010; Mion *et al.*, 2010)—results in a loss of input to language areas that are not directly lesioned. One important point to highlight is that the current study, with a sufficient number of patients for its goal of mapping the white matter tract involvement in semantic dementia, lacked sufficient power to run covariate analyses with behavioural data. Whether damage to this pathway linking the ventrorostral temporal area to lateral parietotemporal language areas is enough to explain the entirety of the language abnormality in semantic dementia, or whether there are also important contributions through uncinate and arcuate bundles, remains to

be determined when a larger cohort of patients has been assessed with this imaging protocol.

An interesting negative in the present study was the absence of parahippocampal white matter damage. In stark contrast to the earlier study of Alzheimer's disease employing this same paradigm (Acosta-Cabronero *et al.*, 2010), abnormality of this region involved only a small rostral area subjacent to the hippocampal head that did not track back towards the cingulum. This is consistent with the known rostral bias of hippocampal atrophy in semantic dementia (Chan *et al.*, 2001; Nestor *et al.*, 2006). Considering the severity of hippocampal atrophy in semantic dementia (Galton *et al.*, 2001; Davies *et al.*, 2004), however, it is also somewhat surprising. Given the qualitative differences in the cognitive profile of semantic dementia and Alzheimer's disease, a final point of interest is that the present semantic dementia study and the previous Alzheimer's disease study, using identical acquisition and analysis methods, yielded almost mutually exclusive differences in the topography of white matter degeneration for these two disorders.

As voxel-wise analysis of diffusion tensor imaging data is a relatively new and evolving method, a few technical points warrant discussion. First is the observation that, to visualize long-tract involvement, one has to relax the statistical threshold. We emphasize that this procedure was not exploratory but rather, was motivated by the intent to examine tracts receiving projections from the initial, statistically stringent analysis. Although disease severity and sample size will influence the extent to which abnormal tracts can be visualized, the nature of white matter anatomy means that one should expect the statistical effect to diminish as one moves away from a lesion, because the tracts will contain a progressively diminishing proportion of fibres from the abnormal region. The second point is the observation in the present study that radial diffusivity was the most sensitive metric of white matter change. Previously we reported, using precisely the same acquisition protocol in Alzheimer's disease, that radial diffusivity and λ_1 were broadly concordant (though with a slight increase in sensitivity for λ_1); for the derived metrics, this meant that mean diffusivity was also sensitive, but fractional anisotropy was not (Acosta-Cabronero *et al.*, 2010). In the current study, however, disproportionate radial diffusivity changes enabled fractional anisotropy to capture white matter alterations in semantic dementia. The conclusion from this contrast is that one cannot assume a universal diffusion metric that should be applied equally in all circumstances. This is not surprising given that factors such as apoptosis and glial pathology differ in different pathologies, and that these may affect the tensor behaviour in different ways. The contrast of Alzheimer's disease and semantic dementia pathologies highlights the critical importance of exploring the full tensor, in particular to avoid the risk of false-negative results. Whether this differential involvement of tensor metrics could have any diagnostic specificity remains to be seen.

In conclusion, results from this diffusion tensor imaging study of 10 patients with semantic dementia join findings from structural and functional imaging in this disease to tell a coherent story regarding the neural basis for the severe and relatively selective deficit of semantic knowledge in semantic dementia. Furthermore, our results indicate that ventrorostral temporal lobe degeneration causes loss of axonal projections to the 'classic' post-Rolandic language areas and to the arcuate and uncinate bundles.

Acknowledgements

We are grateful for the support from our patients and healthy volunteers.

Funding

Medical Research Council, UK (to P.J.N. and J.R.H); National Institute for Health Research, Cambridge Biomedical Research Centre, UK (to P.J.N.); Alzheimer's Research UK (to J.A.-C. and G.P.); Leverhulme Trust (to K.P.); and Australian Research Council (to J.R.H).

References

Acosta-Cabronero J, Williams GB, Pengas G, Nestor PJ. Absolute diffusivities define the landscape of white matter degeneration in Alzheimer's disease. Brain 2010; 133: 529–39.

Acosta-Cabronero J, Williams GB, Pereira JM, Pengas G, Nestor PJ. The impact of skull-stripping and radio-frequency bias correction on grey-matter segmentation for voxel-based morphometry. Neuroimage 2008; 39: 1654–65.

Adlam AL, Patterson K, Rogers TT, Nestor PJ, Salmond CH, Acosta-Cabronero J, et al. Semantic dementia and fluent primary progressive aphasia: two sides of the same coin? Brain 2006; 129: 3066–80.

Agosta F, Henry RG, Migliaccio R, Neuhaus J, Miller BL, Dronkers NF, et al. Language networks in semantic dementia. Brain 2010; 133: 286–99.

Ashburner J, Friston KJ. Voxel-based morphometry–the methods. Neuroimage 2000; 11: 805–21.

Ashburner J, Friston KJ. Unified segmentation. Neuroimage 2005; 26: 839–51.

Behrens TE, Berg HJ, Jbabdi S, Rushworth MF, Woolrich MW. Probabilistic diffusion tractography with multiple fibre orientations: what can we gain? Neuroimage 2007; 34: 144–55.

Behrens TE, Johansen-Berg H, Woolrich MW, Smith SM, Wheeler-Kingshott CA, Boulby PA, et al. Non-invasive mapping of connections between human thalamus and cortex using diffusion imaging. Nat Neurosci 2003a; 6: 750–7.

Behrens TE, Woolrich MW, Jenkinson M, Johansen-Berg H, Nunes RG, Clare S, et al. Characterization and propagation of uncertainty in diffusion-weighted MR imaging. Magn Reson Med 2003b; 50: 1077–88.

Binney RJ, Embleton KV, Jefferies E, Parker GJ, Lambon Ralph MA. The ventral and inferolateral aspects of the anterior temporal lobe are crucial in semantic memory: evidence from a novel direct comparison of distortion-corrected fMRI, rTMS, and semantic dementia. Cereb Cortex 2010; 20: 2728–38.

Bozeat S, Lambon Ralph MA, Patterson K, Garrard P, Hodges JR. Non-verbal semantic impairment in semantic dementia. Neuropsychologia 2000; 38: 1207–15.

Catani M, Jones DK, ffytche DH. Perisylvian language networks of the human brain. Ann Neurol 2005; 57: 8–16.

Chan D, Fox NC, Scahill RI, Crum WR, Whitwell JL, Leschziner G, et al. Patterns of temporal lobe atrophy in semantic dementia and Alzheimer's disease. Ann Neurol 2001; 49: 433–42.

Davies RR, Graham KS, Xuereb JH, Williams GB, Hodges JR. The human perirhinal cortex and semantic memory. Eur J Neurosci 2004; 20: 2441–6.

Desgranges B, Matuszewski V, Piolino P, Chetelat G, Mezenge F, Landeau B, et al. Anatomical and functional alterations in semantic dementia: a voxel-based MRI and PET study. Neurobiol Aging 2007; 28: 1904–13.

Fein G, Landman B, Tran H, Barakos J, Moon K, Di Sclafani V, et al. Statistical parametric mapping of brain morphology: sensitivity is dramatically increased by using brain-extracted images as inputs. Neuroimage 2006; 30: 1187–95.

Folstein MF, Folstein SE, McHugh PR. "Mini-mental state". A practical method for grading the cognitive state of patients for the clinician. J Psychiatr Res 1975; 12: 189–98.

Galton CJ, Patterson K, Graham K, Lambon-Ralph MA, Williams G, Antoun N, et al. Differing patterns of temporal atrophy in Alzheimer's disease and semantic dementia. Neurology 2001; 57: 216–25.

Graham KS, Simons JS, Pratt KH, Patterson K, Hodges JR. Insights from semantic dementia on the relationship between episodic and semantic memory. Neuropsychologia 2000; 38: 313–24.

Griswold MA, Jakob PM, Heidemann RM, Nittka M, Jellus V, Wang J, et al. Generalized autocalibrating partially parallel acquisitions (GRAPPA). Magn Reson Med 2002; 47: 1202–10.

Hodges JR, Martinos M, Woollams AM, Patterson K, Adlam AL. Repeat and point: differentiating semantic dementia from progressive non-fluent aphasia. Cortex 2008; 44: 1265–70.

Hodges JR, Mitchell J, Dawson K, Spillantini MG, Xuereb JH, McMonagle P, et al. Semantic dementia: demography, familial factors and survival in a consecutive series of 100 cases. Brain 2010; 133: 300–6.

Hodges JR, Patterson K, Oxbury S, Funnell E. Semantic dementia. Progressive fluent aphasia with temporal lobe atrophy. Brain 1992; 115 (Pt 6): 1783–806.

Ikeda M, Patterson K, Graham KS, Lambon Ralph MA, Hodges JR. A horse of a different colour: do patients with semantic dementia recognise different versions of the same object as the same? Neuropsychologia 2006; 44: 566–75.

Jenkinson M, Smith S. A global optimisation method for robust affine registration of brain images. Med Image Anal 2001; 5: 143–56.

Kinahan PE, Rogers JG. Analytic 3D image reconstruction using all detected events. IEEE Trans Nucl Sci 1989; 36: 964–8.

Marinkovic K, Dhond RP, Dale AM, Glessner M, Carr V, Halgren E. Spatiotemporal dynamics of modality-specific and supramodal word processing. Neuron 2003; 38: 487–97.

McKenna P, Warrington EK. The graded naming test. Windsor, UK: NFER-Nelson; 1983.

Mion M, Patterson K, Acosta-Cabronero J, Pengas G, Izquierdo-Garcia D, Hong YT, et al. What the left and right anterior fusiform gyri tell us about semantic memory. Brain 2010; 133: 3256–68.

Mioshi E, Dawson K, Mitchell J, Arnold R, Hodges JR. The Addenbrooke's Cognitive Examination Revised (ACE-R): a brief cognitive test battery for dementia screening. Int J Geriatr Psychiatry 2006; 21: 1078–85.

Neary D, Snowden JS, Gustafson L, Passant U, Stuss D, Black S, et al. Frontotemporal lobar degeneration: a consensus on clinical diagnostic criteria. Neurology 1998; 51: 1546–54.

Nestor PJ, Fryer TD, Hodges JR. Declarative memory impairments in Alzheimer's disease and semantic dementia. Neuroimage 2006; 30: 1010–20.

Osterrieth PA. Filetest de copie d'une figure complex: contribution a l'etude de la perception et de la memoire [The test of copying a complex figure: a contribution to the study of perception and memory]. Arch Psychol 1944; 30: 206–56.

Patterson K, Nestor PJ, Rogers TT. Where do you know what you know? The representation of semantic knowledge in the human brain. Nat Rev Neurosci 2007; 8: 976–87.

Pengas G, Patterson K, Arnold RJ, Bird CM, Burgess N, Nestor PJ. Lost and found: bespoke memory testing for Alzheimer's disease and semantic dementia. J Alzheimers Dis 2010; 21: 1347–65.

Pereira JM, Williams GB, Acosta-Cabronero J, Pengas G, Spillantini MG, Xuereb JH, et al. Atrophy patterns in histologic vs clinical groupings of frontotemporal lobar degeneration. Neurology 2009; 72: 1653–60.

Pereira JM, Xiong L, Acosta-Cabronero J, Pengas G, Williams GB, Nestor PJ. Registration accuracy for VBM studies varies according to region and degenerative disease grouping. Neuroimage 2010; 49: 2205–15.

Reese TG, Heid O, Weisskoff RM, Wedeen VJ. Reduction of eddy-current-induced distortion in diffusion MRI using a twice-refocused spin echo. Magn Reson Med 2003; 49: 177–82.

Rueckert D, Sonoda LI, Hayes C, Hill DLG, Leach MO, Hawkes DJ. Non-rigid registration using free-form deformations: application to breast MR images. IEEE Trans Med Imaging 1999; 18: 712–21.

Segonne F, Dale AM, Busa E, Glessner M, Salat D, Hahn HK, et al. A hybrid approach to the skull stripping problem in MRI. Neuroimage 2004; 22: 1060–75.

Sled JG, Zijdenbos AP, Evans AC. A nonparametric method for automatic correction of intensity nonuniformity in MRI data. IEEE Trans Med Imaging 1998; 17: 87–97.

Smith SM. Fast robust automated brain extraction. Hum Brain Mapp 2002; 17: 143–55.

Smith SM, Jenkinson M, Johansen-Berg H, Rueckert D, Nichols TE, Mackay CE, et al. Tract-based spatial statistics: voxelwise analysis of multi-subject diffusion data. Neuroimage 2006; 31: 1487–505.

Smith SM, Jenkinson M, Woolrich MW, Beckmann CF, Behrens TE, Johansen-Berg H, et al. Advances in functional and structural MR image analysis and implementation as FSL. Neuroimage 2004; 23 (Suppl 1): S208–19.

Smith SM, Nichols TE. Threshold-free cluster enhancement: addressing problems of smoothing, threshold dependence and localisation in cluster inference. Neuroimage 2009; 44: 83–98.

Snowden JS, Goulding PJ, Neary D. Semantic dementia: a form of circumscribed cerebral atrophy. Behav Neurol 1989; 2: 167–82.

Ture U, Yasargil MG, Friedman AH, Al-Mefty O. Fiber dissection technique: lateral aspect of the brain. Neurosurgery 2000; 47: 417–26; discussion 426–7.

Vigneau M, Beaucousin V, Herve PY, Duffau H, Crivello F, Houde O, et al. Meta-analyzing left hemisphere language areas: phonology, semantics, and sentence processing. Neuroimage 2006; 30: 1414–32.

Whitwell JL, Avula R, Senjem ML, Kantarci K, Weigand SD, Samikoglu A, et al. Gray and white matter water diffusion in the syndromic variants of frontotemporal dementia. Neurology 2010; 74: 1279–87.